Hindawi Publishing Corporation
International Journal of Microwave Science and Technology
Volume 2012, Article ID 375601, 7 pages
doi:10.1155/2012/375601

Research Article

Complex Permittivity Measurements of Textiles and Leather in a Free Space: An Angular-Invariant Approach

B. Kapilevich, B. Litvak, M. Anisimov, D. Hardon, and Y. Pinhasi

Department Electrical and Electronics Engineering, Ariel University Center of Samaria, Ariel 40700, Israel

Correspondence should be addressed to B. Kapilevich, boriskap@ariel.ac.il

Received 5 March 2012; Accepted 15 May 2012

Academic Editor: Andrea Randazzo

The paper describes the complex permittivity measurements of textiles and leathers in a free space at 330 GHz. The destructive role of the Rayleigh scattering effect is considered and the angular-invariant limit for an incidence angle has been found out experimentally within 25–30 degrees. If incidence angle exceeds this critical parameter, the uncertainty caused by the Rayleigh scattering is drastically increased preventing accurate measurements of the real and imaginary parts of a bulky material. The phenomenon must be taken into consideration in predicting shielding effectiveness of materials covering hidden object in concealed threat detection with millimeter-wave radar systems.

1. Introduction

Submillimeter and THz waves demonstrate a reasonable penetration depth in certain common materials, such as fabric, plastic, and wood. Therefore, they are good candidates for detecting various hidden objects such as concealed weapons, drags, and explosives. In the last decade, there has been a growing demand in mm, sub-mm, and THz imaging systems for homeland security applications [1, 2]. In particular, efficiency of these systems depends on shielding effectiveness of materials screening the detected object [3].

Complex permittivity $\varepsilon(f)$ is widely used for characterization of dielectric materials. It is frequency-dependent quantity, resulting in attenuation and phase shifts of electromagnetic wave propagating in media. In a slab structure, the permittivity can be acquired from the transmission and reflection coefficients. Knowledge of the dielectric properties of these materials is important in predicting overall performance of mm-wave imagers because a penetration depth is governed by these characteristics. There are a lot of microwave methods suggested for measuring complex permittivity [4], but free-space approach is more suitable in sub-mm range since the sample size has reasonable dimensions in order to avoid undesirable edge diffraction effect. However, the drawback of most free-space measuring systems is the ripples (or parasitic resonances) in the measured data caused by multiple reflections from sample surfaces and antennas that cannot be accurately predicted in the theoretical models. As a result, various smoothing algorithms based on heuristic criteria must be used to overcome degrading measurement accuracy [5, 6].

An isotropic slab in air [7] is the basic theoretical model employed for retrieving the complex permittivity from the measured data. However, approximation of textiles having typical woven fabric nature and leather materials with nonregular surface's shaping by uniform dielectric slab is incorrect. Indeed, texture and surface roughness maybe comparable with wavelength and responsible for the Rayleigh scattering that may drastically degrade the measurement accuracy. One to overcome the problem is the development of special data smoothing algorithms [8] needed to avoid undesirable rapid oscillations caused by the parasitic standing wave interference between R_x and T_x antennas as well as other factors. As a result, the originally measured transmittance cannot be used for validation of the best-fitting permittivity without additional specific processing.

Assuming that textiles and leathers are isotropic materials, they must have invariant values of complex permittivity regardless of an incidence angle. The deviations of real and imaginary parts of the dielectric constant can be considered as a measure of a nonuniformity of the thickness and

surface's shape of the dielectric slab approximating a real sample. This parameter has statistical nature and should be characterized by standard deviation of the measured material characteristics in angular domain. In the present study, the matched THz power meter (MPM) has been used in the transmittance measurements at 330 GHz resulting in a minimization of destructive role of the parasitic standing wave interference [9]. High directivity Gaussian beam horn-lens antenna was employed in order to suppress undesirable spillover effect during variations of the sample's position.

2. Theoretical Basis of the Model

Assume that dielectric slab of thickness d is illuminated by plane wave with incident angle θ_0. The field reflection r and transmission t coefficients being basic physical parameters measured in free-space method can be presented in general form via proper Fresnel's formulas [10] as nonlinear functions of d, θ_0, the frequency f, and the relative complex dielectric constant $\varepsilon_r' - j\varepsilon_r''$:

$$t = \frac{\left(1-\rho_0^2\right)\, e^{-jk_z(f)d}}{1-\rho_0^2 e^{-j2k_z(f)d}} = \frac{\left(1-\rho_0^2\right)\, e^{-(\alpha+j\beta)\cos(\theta)d}}{1-\rho_0^2 e^{-2(\alpha+j\beta)\cos(\theta)d}},$$
$$r = \rho_0 \cdot \frac{1-e^{-j2k_z(f)d}}{1-\rho_0^2 e^{-j2k_z(f)d}} = \rho_0 \cdot \frac{1-e^{-2(\alpha+j\beta)\cos(\theta)d}}{1-\rho_0^2 e^{-2(\alpha+j\beta)\cos(\theta)d}}, \tag{1}$$

where

$$\rho_0 = \begin{cases} \dfrac{\sqrt{\varepsilon_0}\cos(\theta_0) - \sqrt{\varepsilon_r}\cos(\theta)}{\sqrt{\varepsilon_0}\cos(\theta_0) + \sqrt{\varepsilon_r}\cos(\theta)} & \text{TE wave} \\ \dfrac{\sqrt{\varepsilon_0}\cos(\theta) - \sqrt{\varepsilon_r}\cos(\theta_0)}{\sqrt{\varepsilon_0}\cos(\theta) + \sqrt{\varepsilon_r}\cos(\theta_0)} & \text{TM wave.} \end{cases} \tag{2}$$

According to the generalized Snell's law, we can write the following for lossy dielectric medium:

$$tg(\theta) = \frac{\sin(\theta_0)}{\operatorname{Re}\left\{\sqrt{\underbrace{\left(\varepsilon' - j\varepsilon''\right)}_{\varepsilon_r} - \sin^2(\theta_0)}\right\}}. \tag{3}$$

If the experimental setup is equipped by a vector network analyzer (VNA), the magnitude and phase of r and t can be measured. Otherwise the power transmission and reflection coefficients are available only

$$|t|^2 = \frac{\left(1-\rho_0^2\right)^2 e^{-2\alpha\cos(\theta)d}}{\left[1-\rho_0^2 e^{-2\alpha\cos(\theta)d}\right]^2 + 4\rho_0^2 e^{-2\alpha\cos(\theta)d}\sin^2\left[\beta\cos(\theta)d\right]},$$
$$|r|^2 = \rho_0^2 \cdot \frac{\left[1-e^{-2\alpha\cos(\theta)d}\right]^2 + 4e^{-2\alpha\cos(\theta)d}\sin^2\left[\beta\cos(\theta)d\right]}{\left[1-\rho_0^2 e^{-2\alpha\cos(\theta)d}\right]^2 + 4\rho_0^2 e^{-2\alpha\cos(\theta)d}\sin^2\left[\beta\cos(\theta)d\right]}. \tag{4}$$

The real and imaginary parts of the dielectric constant as a function of incidence angle were evaluated from the measured transmittance using the numerical root-finding algorithm applied to the system of nonlinear equations:

$$\left|t(f,d,\theta_1,\varepsilon_r',\varepsilon_r'')\right|^2 = T_{p1},$$
$$\left|t(f,d,\theta_2,\varepsilon_r',\varepsilon_r'')\right|^2 = T_{p2}, \tag{5}$$

where T_{p1} and T_{p2} are power transmission coefficients measured at the incidence angles θ_1 and θ_2, respectively, d is the thickness of a dielectric slab. Then, the proper standard deviations were determined for textile and leather samples in order to characterize angular invariances of the measured parameters. This model is used below for extracting complex permittivity from the measured data.

3. The Experimental Setup

In order to avoid an undesirable cross-polarization effect, all the measurements are suggested to perform with a parallel polarization, for which MPM is well matched as it is operating near the Brewster angle of the absorbing RF power thin-film sensor as shown in Figure 1. For absorbing thin film element of the power meter (Thomas Keating THz Power Meter, http://www.terahertz.co.uk/) this angle is equal to 55.5 degrees. The input window of the power meter must be aligned at the Brewster angle in order to reach the best matching condition.

Figure 2 shows the photo of the experimental setup assembled for the material characterization near f = 330 GHz. The THz source consists of the X-Band Synthesizer with power amplifier at its output that drives multistage multiplier (4 sections) with the total multiplication factor $32 = 4 \times 2 \times 2 \times 2$. Output signal about 10 mW is radiated by the horn-lens antenna (1.3 deg beam width and 42 dB gain). Other details concerning the source can be found in [1]. Energy propagating through the dielectric slab is captured by absorbing thin film of THz power meter and after processing is displayed on the PC monitor. The tested material is fixed by special frame maintained on programmable rotary joint model URS-75-BPP (Newport).

The measurement procedure includes the two steps:

(i) calibration-measurement of the transmitted signal without material under test (P_0);

(ii) measurements of the transmitted signal as a function of incident angle in a presence of material under test (P_1);

the ratio P_1/P_0 is the power transmittance needed to extract the complex permittivity.

4. Results of Transmittance Measurements and Reconstruction Complex Permittivity

Several types of the textiles have been tested. The specifications of these materials are summarized in the Table 1. Also,

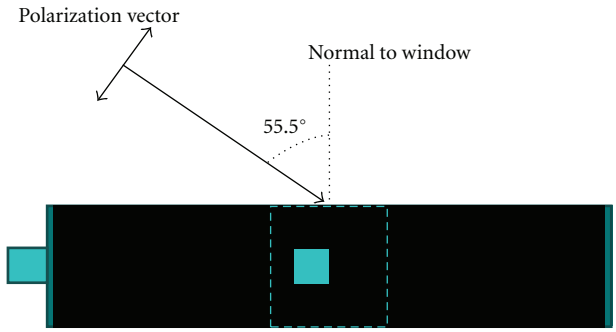

FIGURE 1: The position the MPM's head aligned at the Brewster angle 55.5 degrees to the incoming beam in order to minimize reflections from the input window.

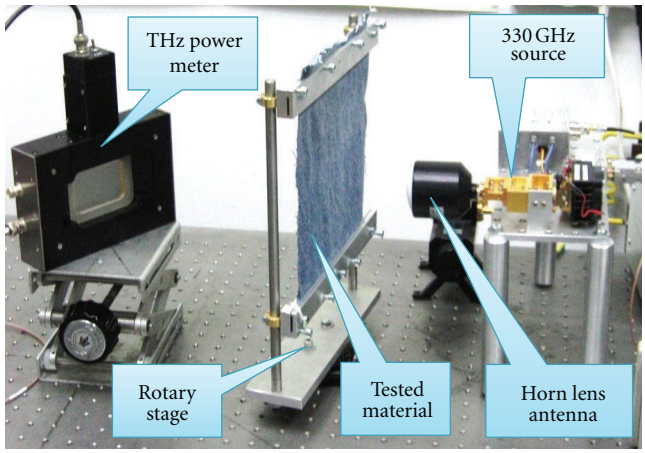

FIGURE 2: Photo of the experimental setup.

several types of leathers have been tested, see Table 2. Figures 3 and 4 show the measured transmittances as a function of incidence angle for textile and leather samples, respectively. The polarization is matched with polarization of the power meter.

The reconstructing procedure needed to restore complex permittivity from the transmittance measurements has been described in [9]. The solution of the system of nonlinear equations (5) requires knowledge of the two independent transmittances for corresponding incidence angles. The latter can be arbitrary but we have fixed one of them assuming that $\theta_1 = 0$ while the second angle was varied in range $5 \le \theta_2 \le 50$ degrees. Tables 3 and 4 summarize the restored real and imaginary parts of dielectric constants of the textile's samples for different incidence angles. The similar data are given in the Tables 5 and 6 for leather's samples.

Both textile and leather samples have demonstrated variations of complex permittivity for different incidence angles due to nonuniform thickness, surface roughness, specific texture and non-ideal flatness. All these factors have statistical nature and can be characterized by standard deviation presented in the last lines of the Tables 3–6.

5. Angular-Invariant Limits of the Incidence Angle

In order to estimate the angular-invariant limits of the incident angle we assume that surface the roughness of textile's and leather's samples satisfies to the Rayleigh scattering condition [11]:

$$\Delta h < \frac{\lambda}{8 \cos \theta_i}, \tag{6}$$

where Δh is roughness variation, θ_i is incidence angle, and λ is free space wavelength. Figure 5 illustrates schematically forward scattered rays "generated" by roughness surface.

Since the roughness variation Δh and incidence angle θ_i are interrelated due to expression (6), we can expect that the uncertainty in a determination of the complex permittivity should be increased with increasing θ_i, too. The question is what is the acceptable range of incidence angles θ_i invariant to the bulky complex permittivity of the material under test-textile and leather in our case? To answer the question we need to compare the measured transmittance of a real material having rough surface with the calculated transmittance of the smoothed dielectric slab made from the same bulky material. The results of such comparison are shown in Figure 6 (textile's sample number 3, $\varepsilon_r' = 2.72$ and $\varepsilon_r'' = 0.068$) and Figure 7 (leather's sample number 0, $\varepsilon_r' = 3.4$ and $\varepsilon_r'' = 0.127$), where the lines marked by symbol □□□ correspond to the measured transmittance while the solid lines depict the calculated data. The averaged values of the real and imaginary parts of the dielectric constants given in the Tables 3–6 were substituted to the theoretical model described by (4). The comparison theory and experiments reveals an existence of the critical incidence angle, θ_c. The latter is determined by the angular-invariance limit of the forward Rayleigh scattering as well as operating wavelength. The materials discussed have the critical angles about 25 degrees for leather's sample and 30 degrees for textile's one. If an incidence angle is greater than the critical one ($\theta_i > \theta_c$), the measurement of the bulk permittivity will be quite problematic due to violating the angular-invariant limit. On the other hand, there is a critical roughness variation Δh, too. Using (6), this parameter was found to be equal to about 0.15 mm for operating frequency 330 GHz and $\theta_c = 30°$. These estimates seem to be realistic for the typical kinds of textiles and leathers.

It would be important to derive an existence of the angular-invariant limit from a theoretical model. Such a model must unify both deterministic and statistic properties of real structure of materials under test. Microwave properties of the common weave architectures used in woven fabric structural composites have been investigated in [12] using deterministic approach. Other perspective way is an application of the concept of the fractional Brownian motion appropriately describing natural surfaces [13] assuming that surface profiles can be approximated by the Weierstrass-Mandelbrot (WM) fractal functions. However, some entry parameters needed for real-world calculations such as the

Table 1: The summary of textile's samples under test.

Material	Sample no. 1 (denim)	Sample no. 2	Sample no. 3	Sample no. 4	Sample no. 5	Sample no. 6 (wool scarf)	Sample no. 7 (stockinet)	Sample no. 8 (satin)
General view of samples under testing		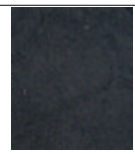						
Thickness d, mm	0.8	0.45	0.25	0.7	0.25	1.6	0.65	0.2
Power transmittance at normal incidence	77%	87%	92%	86%	88.8%	35%	67%	91%

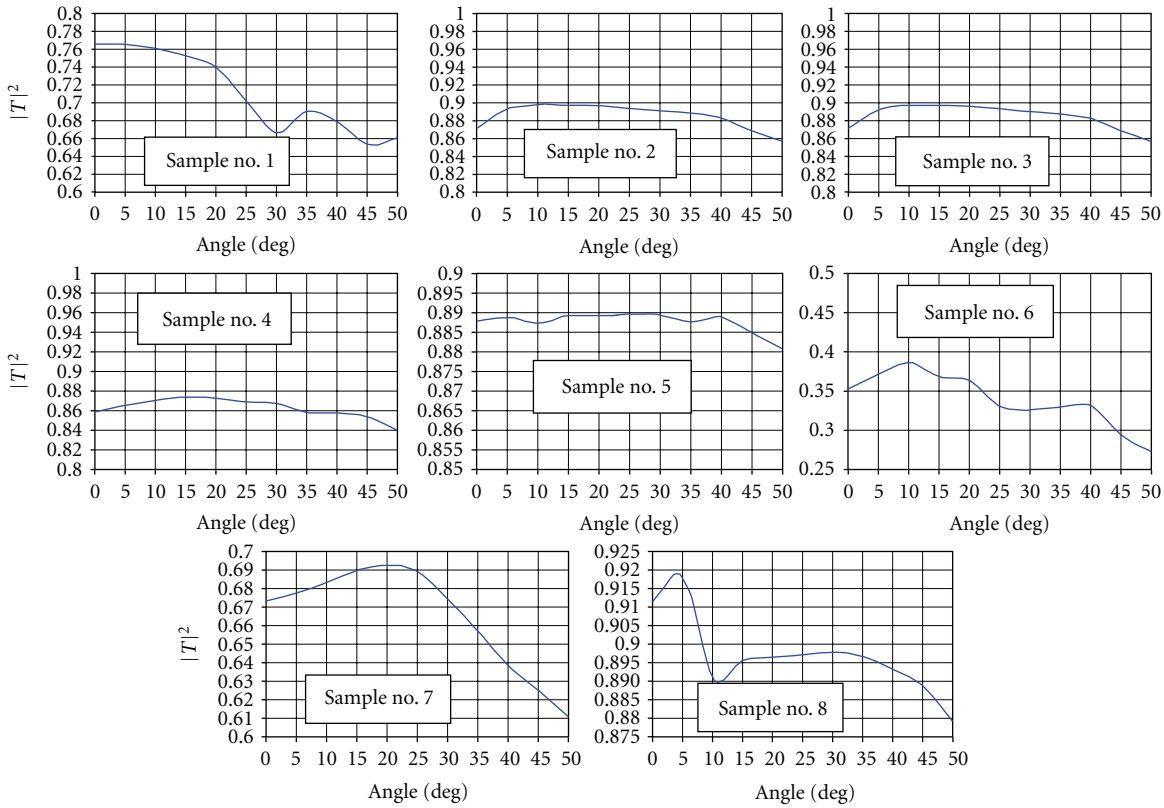

Figure 3: Measured power transmittance of the textile's samples as a function of incidence angle.

Table 2: The summary of leather's samples under test.

Material	Sample no. 0 (natural leather)	Sample no. 1 (artificial leather)	Sample no. 2 (artificial leather)	Sample no. 3 (artificial leather)	Sample no. 4 (artificial leather)	Sample no. 5 (artificial leather)
General view of samples under testing		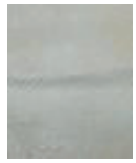		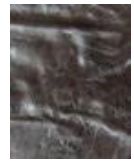	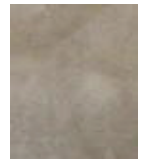	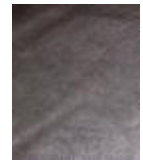
Thickness d, mm	1.15	0.95	1	0.6	0.8	0.6
Power transmittance at normal incidence	48%	63%	68%	81.5%	71%	77%

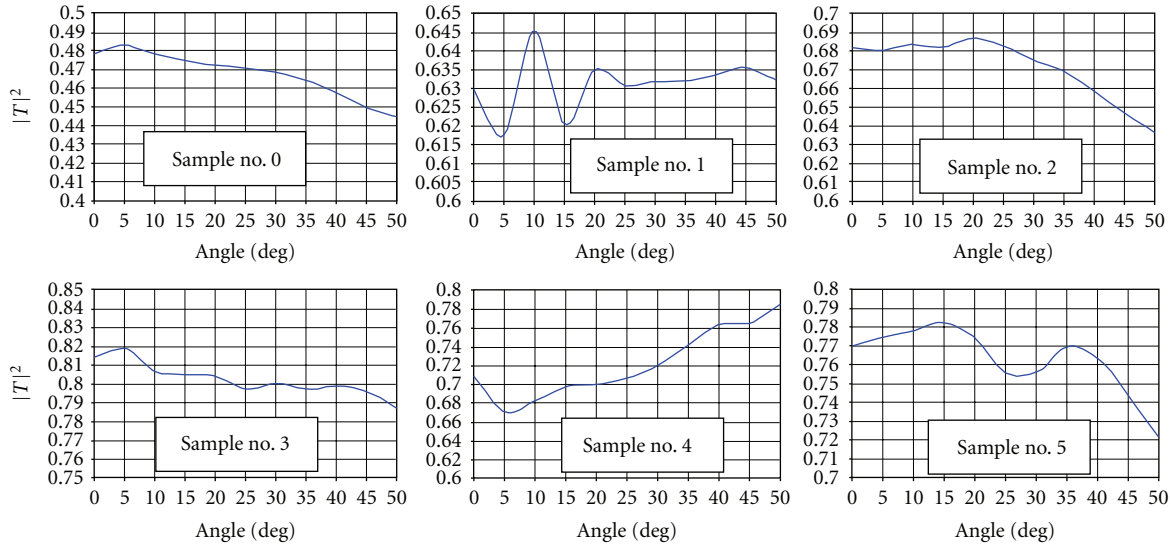

Figure 4: Measured power transmittance of the leather's samples as a function of incidence angle.

Table 3: Real part of the permittivity evaluated for the textile's samples: $\theta_1 = 0$ and different incidence angles θ_2.

Incidence angle, θ_2 degrees	Sample no. 1 (Denim)	Sample no. 2	Sample no. 3	Sample no. 4	Sample no. 5	Sample no. 6 (wool scarf)	Sample no. 7 (stock-inet)	Sample no. 8 (satin)
5	2.83	2.77	2.73	3.65	2.54	3.2	3.15	2.73
10	2.71	2.71	2.7	3.76	2.43	3.21	3.13	2.69
15	2.67	2.92	2.74	3.67	2.41	3.23	3.17	2.73
20	2.7	2.76	2.77	3.67	2.49	3.12	3.17	2.75
25	2.73	2.68	2.79	3.65	2.51	3.11	3.2	2.76
30	2.69	2.5	2.75	3.67	2.54	3.14	3.34	2.75
35	2.67	2.26	2.7	3.66	2.54	3.17	3.34	2.76
40	2.75	2.84	2.75	3.68	2.58	3.2	3.22	2.76
45	2.78	2.95	2.59	3.66	2.68	3.22	3.26	2.75
50	2.79	3.01	2.71	3.58	2.68	3.23	3.21	2.76
Averaged, ε_r'	2.73	2.74	2.72	3.66	2.54	3.18	3.22	2.74
Standard deviation	0.054	0.253	0.0623	0.0458	0.0956	0.0452	0.0737	0.0216

Table 4: Imaginary part of the permittivity evaluated for the textile's samples: $\theta_1 = 0$ and different incidence angles θ_2.

Incidence angle, θ_2 degrees	Sample no. 1 (cotton jeans)	Sample no. 2	Sample no. 3	Sample no. 4	Sample no. 5	Sample no. 6 (wool scarf)	Sample no. 7 (stock-inet)	Sample no. 8 (satin)
5	0.0715	0.033	0.07	0.041	0.065	0.133	0.054	0.074
10	0.0633	0.029	0.057	0.028	0.06	0.13	0.057	0.072
15	0.0603	0.0103	0.06	0.038	0.045	0.134	0.041	0.071
20	0.0634	0.033	0.062	0.043	0.048	0.145	0.042	0.072
25	0.071	0.0397	0.065	0.044	0.052	0.158	0.054	0.072
30	0.0781	0.011	0.068	0.044	0.061	0.159	0.076	0.073
35	0.074	0.011	0.071	0.044	0.072	0.159	0.1	0.074
40	0.079	0.019	0.08	0.043	0.077	0.161	0.119	0.077
45	0.0858	0.06	0.085	0.044	0.089	0.172	0.126	0.08
50	0.0866	0.065	0.069	0.047	0.092	0.175	0.13	0.086
Averaged, ε_r''	0.073	0.031	0.068	0.042	0.066	0.15	0.08	0.075
Standard deviation	0.0092	0.0222	0.0097	0.0056	0.0172	0.0162	0.0356	0.0049

Table 5: Real part of the permittivity evaluated for the leather's samples: $\theta_1 = 0$ and different incidence angles θ_2.

Incidence angle, θ_2 degrees	Sample no. 0	Sample no. 1	Sample no. 2	Sample no. 3	Sample no. 4	Sample no. 5
5	2.91	3.3	2.95	2.18	2.7	2.48
10	3.31	2.97	3.03	2.03	2.71	2.75
15	3.39	3.17	3.03	2.05	2.73	2.66
20	3.42	2.99	3.08	2.16	2.96	2.51
25	3.45	3.02	3.04	2.11	3.03	2.33
30	3.44	3.03	3.05	2.26	3.09	2.45
35	3.46	3.06	3.05	2.28	3.19	2.45
40	3.5	3.12	3.03	2.28	3.23	2.43
45	3.58	3.17	2.9	2.26	3.25	2.43
50	3.54	3.21	2.92	2.13	3.28	2.45
Averaged, ε_r'	3.4	3.104	3.008	2.17	3.02	2.49
Standard deviation	0.178	0.102	0.058	0.094	0.220	0.1221

Table 6: Imaginary part of the permittivity for the leather's samples: $\theta_1 = 0$ and different incidence angles θ_2.

Incidence angle, θ_2 degrees	Sample no. 0	Sample no. 1	Sample no. 2	Sample no. 3	Sample no. 4	Sample no. 5
5	0.118	0.093	0.078	0.066	0.088	0.084
10	0.109	0.072	0.08	0.062	0.086	0.065
15	0.115	0.079	0.081	0.063	0.083	0.075
20	0.118	0.061	0.08	0.066	0.096	0.09
25	0.12	0.067	0.079	0.065	0.096	0.088
30	0.125	0.071	0.079	0.069	0.091	0.088
35	0.131	0.077	0.078	0.069	0.084	0.087
40	0.14	0.083	0.079	0.067	0.076	0.088
45	0.148	0.089	0.079	0.0676	0.0751	0.088
50	0.15	0.098	0.083	0.067	0.069	0.095
Averaged, ε_r''	0.127	0.079	0.08	0.066	0.084	0.085
Standard deviation	0.0135	0.0111	0.0014	0.0023	0.0086	0.0084

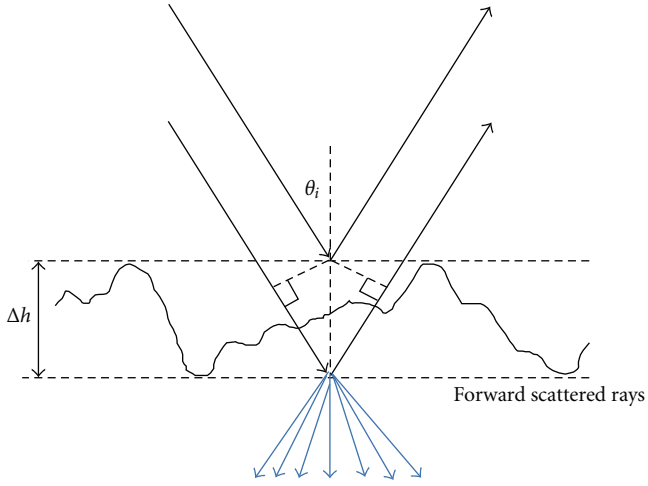

Figure 5: Illustration of the forward Rayleigh scattering effect in presence of a roughness surface.

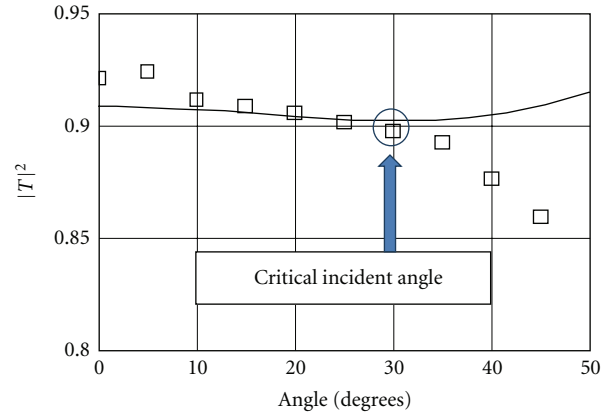

Figure 6: Comparison calculated (solid line) and measured (symbol □□□) transmittances as a function of an incidence angle (the textile's sample #3, $\varepsilon_r' = 2.72$ and $\varepsilon_r'' = 0.068$).

vertical height profile scaling factor, random variables which account for the amplitude, and the phase behavior of each tone, and others [14] must be specified for materials under test which is not trivial problem. Anyway, we hope that the above experiments will be an additional stimulus for developing proper models combining deterministic and statistic approaches, too.

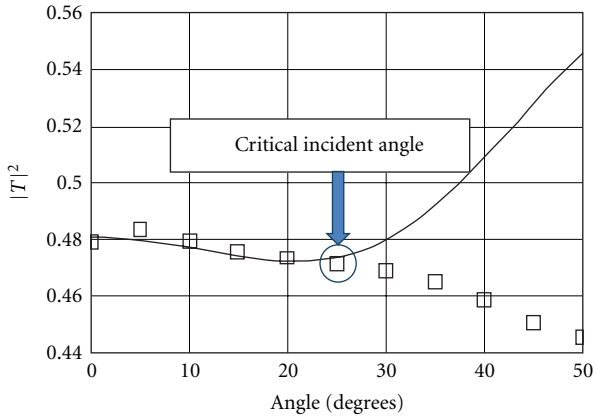

FIGURE 7: Comparison calculated (solid line) and measured (symbol □□□) transmittances as a function of an incidence angle (the leather's sample no. 0, $\varepsilon_r' = 3.4$ and $\varepsilon_r'' = 0.127$).

6. Conclusions

The complex permittivities of textiles and leathers were measured at 330 GHz using the absolute THz power meter with thin-film sensor operating near the Brewster angle in order to provide a minimum multiple-reflection effect. The incidence-angular invariance has been estimated experimentally and existence of a critical incidence angle was found out. It is not recommended to carry out free-space permittivity measurements if the incidence angle exceeds the critical one (25–30 degrees in our case) since the forward Rayleigh scattering effect may drastically degrade the measurement accuracy.

Acknowledgments

Authors would like to thank Dr. J Polivka for fruitful discussions and A. Shulzinger and S. Neporent for assistance in the design and assembling the measuring setup used in the experiments discussed.

References

[1] B. Kapilevich, Y. Pinhasi, R. Arusi et al., "330 GHz FMCW image sensor for homeland security applications," *Journal of Infrared, Millimeter, and Terahertz Waves*, vol. 31, no. 11, pp. 1370–1381, 2010.

[2] B. Kapilevich and M. Einat, "Detecting hidden objects on human body using active millimeter wave sensor," *IEEE Sensors Journal*, vol. 10, no. 11, Article ID 5482043, pp. 1746–1752, 2010.

[3] S. Van den Bulcke, A. Franchois, and D. De Zutter, "2.5 D quantitative millimeter wave imaging of a hidden object on a simplified human body model using value picking regularization," *Journal of Infrared, Millimeter, and Terahertz Waves*, vol. 31, no. 12, pp. 1478–1490, 2010.

[4] L. F. Chen, C. K. Ong, C. P. Neo, V. V. Varadan, and V. K. Varadan, *Microwave Electronics: Measurement and Material Characterization*",, John Wiley & Sons, New York, NY, USA, 2004.

[5] N. Gagnon, J. Shaker, L. Roy, A. Petosa, and P. Berini, "Low-cost free-space measurement of dielectric constant at Ka band," *IEE Proceedings: Microwaves, Antennas and Propagation*, vol. 151, no. 3, pp. 271–276, 2004.

[6] K. M. Hock, "Error correction for diffraction and multiple scattering in free-space microwave measurement of materials," *IEEE Transactions on Microwave Theory and Techniques*, vol. 54, no. 2, pp. 648–659, 2006.

[7] W. D. Burnside and K. W. Burgener, "High frequency scattering by a thin lossless dielectric slab," *IEEE Transactions on Antennas and Propagation*, vol. AP-31, no. 1, pp. 104–110, 1983.

[8] S. W. Harmer, N. Rezgui, N. Bowring, Z. Luklinska, and G. Ren, "Determination of the complex permittivity of textiles and leather in the 14–40 GHz millimetre-wave band using a free-wave transmittance only method IET Microw," *IEEE Transactions on Antennas and Propagation*, vol. 2, no. 6, pp. 606–614, 2008.

[9] B. Kapilevich, Y. Pinhasi, and B. Litvak, "Measurement of complex permittivity of lossy materials in free space using matched THz power meter?" *The International Journal on Infrared Millimeter THz Waves*, vol. 32, no. 12, pp. 1446–1456, 2011.

[10] S. V. Marshall and G. G. Skitek, *Electromagnetic Concepts and Applications*, Prentice-Hall, New York, NY, USA, 2nd edition, 1987.

[11] S. R. Saunders and A. Aragon-Zavala, *Antennas and Propagation for Wireless Communication Systems*, John Wiley, New York, NY, USA, 2007.

[12] M. S. Mirotznik, S. Yarlagadda, R. McCauley, and P. Pa, "Broadband electromagnetic modeling of woven fabric composites," *IEEE Transactions on Microwave Theory and Techniques*, vol. 60, no. 1, pp. 158–169, 2012.

[13] B. B. Mandelbrot, *The Fractal Geometry of Nature*, W. H. Freeman, New York, NY, USA, 1983.

[14] G. Franceschetti, A. Iodice, D. Riccio, and G. Ruello, "Fractal surfaces and electromagnetic extended boundary conditions," *IEEE Transactions on Geoscience and Remote Sensing*, vol. 40, no. 5, pp. 1018–1031, 2002.